RSC Advances

ROYAL SOCIETY OF CHEMISTRY

www.rsc.org/advances

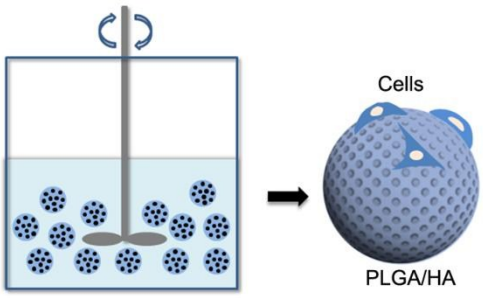

Design macroporous topography on spherical substrates via a straightforward approach and investigate the corresponding cell responses.

RSC Advances

RSCPublishing

ARTICLE

Engineering poly(lactic-co-glycolic acid)/ hydroxyapatite microspheres with diverse macropores patterns and the cellular responses

D. Cheng,[a,b] X. Cao,[*a,b,c] H. Gao,[a,b] J. Hou,[a,b] W. Li,[a,b] L. Hao[a,b] and Y. Wang [*a,b,c]

Cite this: DOI: 10.1039/x0xx00000x

Received 00th January 2012,
Accepted 00th January 2012

DOI: 10.1039/x0xx00000x

www.rsc.org/

Present studies on topographic effects of substrates on cell functions are limited to planar substrates, which are usually not applicable in bone repair. Specific patterns are rarely constructed on 3D substrates. Here spherical substrates with macroporous topography were obtained to explore cellular responses. Macropores with tunable density were generated on the surfaces of poly(lactic-co-glycolic acid)/hydroxyapatite (PLGA/HA) microspheres via using HA particles as the pore-forming source. Different densities of macropores represented different topographies and were found to influence the morphology, proliferation and osteogenic differentiation of human fetal mesenchymal stem cells (fMSCs). The microsphere with medium density of macropores most benefitted proliferation and differentiation of fMSCs compared with the low and high density. This study reveals the role of macroporous spherical surfaces in affecting cell functions and may guide the design of functional substrates in bone repair.

1. Introduction

Native cells are located in a 3D environment known as extracellular matrix (ECM). In tissue repair, it is increasingly recognized that artificial substrates should mimic the function of ECM so as to facilitate cell behaviours.[1] Surface properties play an important role in the performance of the substrates. Besides factors such as surface chemistry and hydrophilicity, the topographic effects on cell behaviours have been well proved.[2, 3] Abundant studies on cell/topography interactions have proved that micro- and nano-scale topographic cues can direct cell fate, including orientation, adhesion, proliferation, and even phonotype of stem cells.[4, 5] Pores are the essential feature for substrates used in tissue engineering. Topographic pits or macropores patterns have also been demonstrated to remarkably influence the cellular behaviours. For instance, pits (0.45 and 2.2 μm in diameter) on polystyrene can improve the adhesion of osteoblast-like cells when compared with the smooth surface.[6] Proliferation, protein synthesis and ALP activity of osteoblast-like cells on polycarbonate further respond to the size of macropores (0.2-8.0 μm).[7] Attachment, motility and proliferation of fibroblasts are also reported to depend on the diameter (7, 15 and 25 μm) and spacing (20-40 μm) of macropores array on poly(L-lactide).[8]

Functional microspheres with specific structures or 'smart' responses have gained wild applications in traditional industry, and increasingly in modern technologies and biomedicine.[9-11] In particular, biodegradable polymer microspheres have attracted great attention in tissue repair, especially in bone repair.[12-14] They are good drug delivery vehicles, as well as easy to prepare and be regulated. Given that human bone is chemically a composite mainly composed of collagen and hydroxyapatite (HA), polymer/HA hybrid microspheres are preferred.[15] Polymer/HA microspheres having enhanced osteoconductivity can be injected or built into 3D scaffold.

As to cells-contacting microspheres, a favorable substrate-cell interaction is critical to *in vivo* success.[16, 17] However, so far, the overwhelming majority of studies with respect to the topographic cues are conducted on planar substrates like films and discs. These substrates are usually not applicable in tissue repair, especially as 3D scaffold for bone repair.[18] And the model cells are confined to osteoblast-like cells or fibroblasts when it comes to pits or macropores patterns.[6-8] Promising stem cells are barely studied. Taking into account the growing application of microspheres and the role of stem cells in bone repair, it is of great use to explore the topographic effects of microspheres on stem cells. Unfortunately, this area is rarely dealt with. This is probably because it is highly challenging to create uniform topography on spherical surface at current level of micromaching.

Here we designed a hybrid PLGA/HA microsphere with arrays of superficial macropores via a straightforward emulsion technique (Fig. 1a). The HA component acted as the pore-forming source (Fig. 1b). The topographic effects of the spherical substrates on adhesion, proliferation and osteogenic differentiation of human fetal mesenchymal stem cells (fMSCs) were investigated in detail (Fig. 1c).

2. Materials and methods

2.1. Materials

Poly(lactic-co-glycolic acid) (PLGA, 50/50, M_w=31 kDa) was purchased from Daigang Biomaterials (Shandong, China). Nano- and micro-hydroxyapatites (HA), poly(vinyl alcohol) (PVA, 87-89% hydrolyzed, Mw=88 kDa) and gluconic acid lactone (GDL) were obtained from Aladdin Chemistry (Shanghai, China). Dichloromethane was bought from Chemical Reagent Factory (Guangzhou, China).

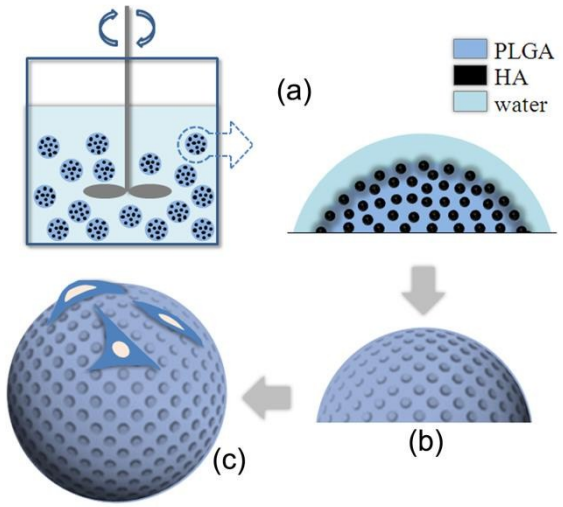

Fig. 1 Illustration of preparing PLGA/HA microspheres with arrays of macropores for cell culture. (a) The PLGA/HA oil droplet in s/o/w emulsion; the HA tended to capture water. (b) Macropores were formed after drying. (c) fMSCs were cultured on the microspheres.

2.2. Preparation of PLGA/HA Microspheres

PLGA/HA microspheres were prepared via emulsion solvent evaporation technique. PLGA was dissolved in dichloromethane (1/10, w/v), followed by the addition of HA particulates. Then the mixture was subject to alternative stirring and ultrasonication to form a homogeneous s/o oil slurry. The slurry was added under stirring into a 0.3% (w/v) PVA and 0.2% GDL (w/v) aqueous solution to form the s/o/w emulsion. Stirring was continued at 300 rpm in fume hood for 8 h to remove the organic solvent. The solidified microspheres were collected, washed with deionized water and lyophilized. Three groups of HA particulates were used (20 nm, 4.60 μm and 16.78 μm).

2.3. Characterization of PLGA/HA microspheres

The morphologies of PLGA/HA microspheres were characterized by Quanta 200 (FEI, Netherland). Samples were mounted on metal stub by double-sided tape and sputter-coated with gold using EM SCD 500 (LEICA, Germany). The accelerating voltage was constant at 15 kV.

The composition of the microspheres was characterized by X'Pert Pro diffractometer (PANalytical, Netherland). Samples were exposed to a Cu Kα radiation and a diffraction of 24-36° (2θ) was analyzed.

The actual amount of HA in the hydrid microspheres was analyzed by TG profile using STA 449C (NETZSCH, Germany). The samples were heated from 30 °C to 1000 °C at a rate of 10 °C/min under a dry nitrogen purge of 20 mL/min. The weight as a function of temperature was analyzed using NETZSCH software.

The porosity features of PLGA/HA microspheres were characterized using AutoPore IV 9500 (Micromeritics, USA). Microspheres were sealed in a penetrometer with a 0.3 mL bulb, weighed and subjected to the mercury intrusion. The pore size distribution, median pore diameter and porosity were calculated.

MFP-3D-S AFM (Asylum Research, USA) was used to further obtain the higher resolution details of different PLGA/HA microspheres. Microspheres were fixed on the glass slide by double-sided tape and a 10 μm ×10 μm zone was scanned.

2.4. Evolution of Morphologies with Degradation

Since the adopted polymers are degradable, the change in morphology with degradation was characterized. Microspheres were immersed into PBS (pH=7.4) in glass vial. All vials were placed in an orbital shaker under 75 rpm and 37 °C. At predetermined time-points, microspheres were taken out, washed and lyophilized for SEM observation. The PBS was refreshed every three days.

2.5. Cell Culture on Microspheres

Human fetal mesenchymal stem cells (fMSCs) were bought from Cyagen Biosciences Inc. (USA). Cells were propagated in high glucose DMEM supplemented with pre-selected 10% (v/v) FBS. Microspheres were placed in 48-well plates and sterilized with γ-irradiation at a dose of 25 kGy. Microspheres were pre-wetted with culture medium for 12 h and then 500 μL of hMSCs suspension (1×10^4 cells/mL) were seeded on the microspheres. The cell/microsphere constructs were incubated at 37 °C, 5% CO_2 in a humidified incubator. The culture media were supplemented with 0.1 μM dexamethasone (Sigma, USA), 10 mM β-glycerophosphate (Calbiochem, USA) and 50 μM ascorbic acid (Sigma, USA), and refreshed every two days.

The adhesion of cells cultured on different PLGA/HA microspheres were observed by Quanta 200 SEM (FEI, Netherland). The cell/microsphere constructs were first washed with PBS and fixed by 2.5 % glutaraldehyde at 4 ℃ for 12 h. The cell/microsphere constructs were dehydrated through a series of degraded alcohols before observation.

Cells adhering on microspheres were also observed by confocal laser scanning microscopy (CLSM, Leica TCS SP8, Germany). Cells were washed with PBS and then fixed by 4% formaldehyde. After being permeabilized in 0.1% Triton X-100 PBS for 15 min, cell cytoskeletal filamentous actin and cell nuclei were stained with Phalloidin-FITC probe (AAT Bioquest® Inc, USA) for 60 min and with DAPI (Beyitime, China) for 5 min, respectively.

The number of cells growing on the microspheres was evaluated by Cell Counting Kit-8 (CCK-8, Dojindo Laboratories, Japan) according to the protocol provided by the manufacturer. The OD value at 450 nm was measured using Thermo 3001 microplate reader (Thermo, USA) (n=4).

RT-PCR was conducted to evaluate the osteogenic differentiation of fMSCs on different PLGA/HA microspheres. Total RNA was isolated using HiPure Total RNA Kits (Magentec, China) according to the manufacturer's instructions. The concentration of RNA was determined using NanoDrop 2000 spectrophotometer (Thermo Scientific, USA). The cDNA was synthesized from 0.5 μg of RNA reverse-transcribed using PrimeScript® RT reagent Kit with gDNA Eraser (TaKaRa Biotechnology, Japan) according to the manufacturer's protocol. RT-PCR reactions for alkaline phosphatase (ALP), osteocalcin (OC) and osteopontin (OPN) genes were performed using SYBR green assay (Invitrogen, USA). The corresponding primer sequences were listed as follows: GAPDH (5'-AGAAAAACCTGCCAAATATGAT GAC-3' and 5'-TGGGTGTCGCTGTTGAAGTC-3'), ALP (5'-AGCACTCCCACTTCATCTGGAA-3' and 5'-GAGACCCAA TAGGTAGTCCACATTG-3'), OC (5'-CAGCGAGGTAGTG AAGAGA-3' and 5'-GAAAGCCGATGTGGTCAG-3') and OPN (5'-GCGAGGAGTTGAATGGTG-3' and 5'-CTTGTGG CTGTGGGTTTC-3'). RT-PCR reactions were carried out in

Chromo 4 real time PCR system (Biorad, USA). Samples were initially held at 95 ℃ for 10 min, followed by 40 cycles composed of denaturation at 95 ℃ for 10 s, annealing at 60 ℃ for 20 s and extension at 72 ℃ for 15 s.

3. Results

3.1. Morphologies and formation mechanism of PLGA/HA Microspheres

Fig. 2 showed the morphologies of PLGA/HA microspheres prepared using different sizes of HA. All the three microspheres well retained the spherical shape as seen in the smaller figures. When the size of HA was of 4.60 μm, there were numerous open macropores distributed throughout the surface (Fig. 2a and d). When the used HA was of 17.68 μm, the quantity of the open macropores decreased significantly (Fig. 2b and e). As nano-HA (20 nm) was incorporated, the amount of macropores decreased further. Only a few discreet macropores existed (Fig. 2c and f). The results revealed that morphologies of the PLGA/HA microspheres were susceptible to the size of HA. Thus microspheres with different macroporous surfaces could be achieved. Here we designated the microspheres with high, medium and low densities of macropores as hPH, mPH and lPH, respectively. When no GDL was added into the aqueous phase, the obtained PLGA/HA microspheres were superficially decorated with HA particles (Fig. S1a and b). And most of the macropores were closed. HA particles were embedded within the microsphere and particles around the surface were accompanied with cavities (Fig. S1c).

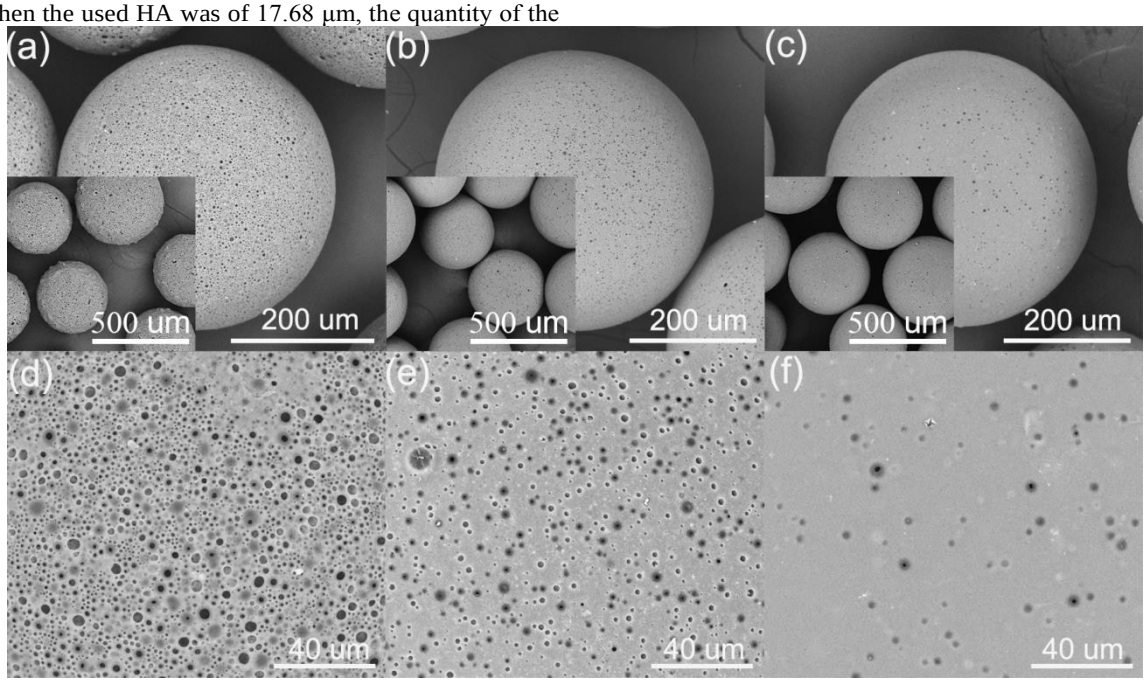

Fig. 2 The SEM images of PLGA/HA microspheres prepared using HA of different sizes. (a and d) Microspheres with high density of macropores (hPH): 4.60 μm; (b and e) microspheres with medium density of macropores (mPH): 17.68 μm; (c and f) microspheres with low density of macropores (lPH): 20 nm. The three small figures were ×150 view.

In Fig. 2, no sign of HA was observed on the surface. XRD analysis was performed to confirm existence of HA in the hybrid microspheres (Fig. 3a). The characteristic peaks at (002), (211), (112), (300) and (202) belonging to HA were clearly identified in the pattern of PLGA/HA microspheres, verifying HA within the microsphere. The amounts of remained HA in different PLGA/HA microspheres were calculated from TG profile (Fig. 3b). The starting mass ratio of HA to PLGA was 0.20. The calculated ratios were 0.173 (HA: 20 nm), 0.164 (HA: 4.60 μm) and 0.147 (HA: 16.78 μm), respectively. This meant that part of HA was consumed during preparation. The largest HA particles lost most; while the smallest ones lost the least.

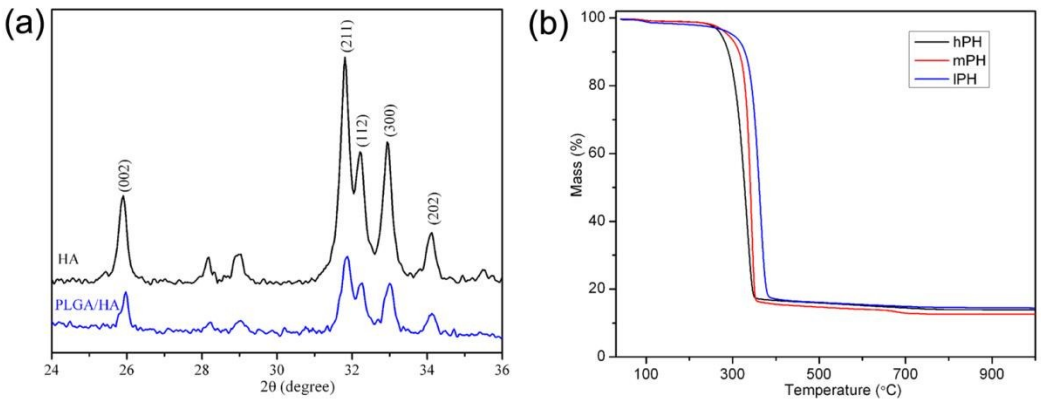

Fig. 3 The XRD patterns (a) of PLGA/HA microsphere and HA particles, and TG profiles (b) of the three PLGA/HA microspheres.

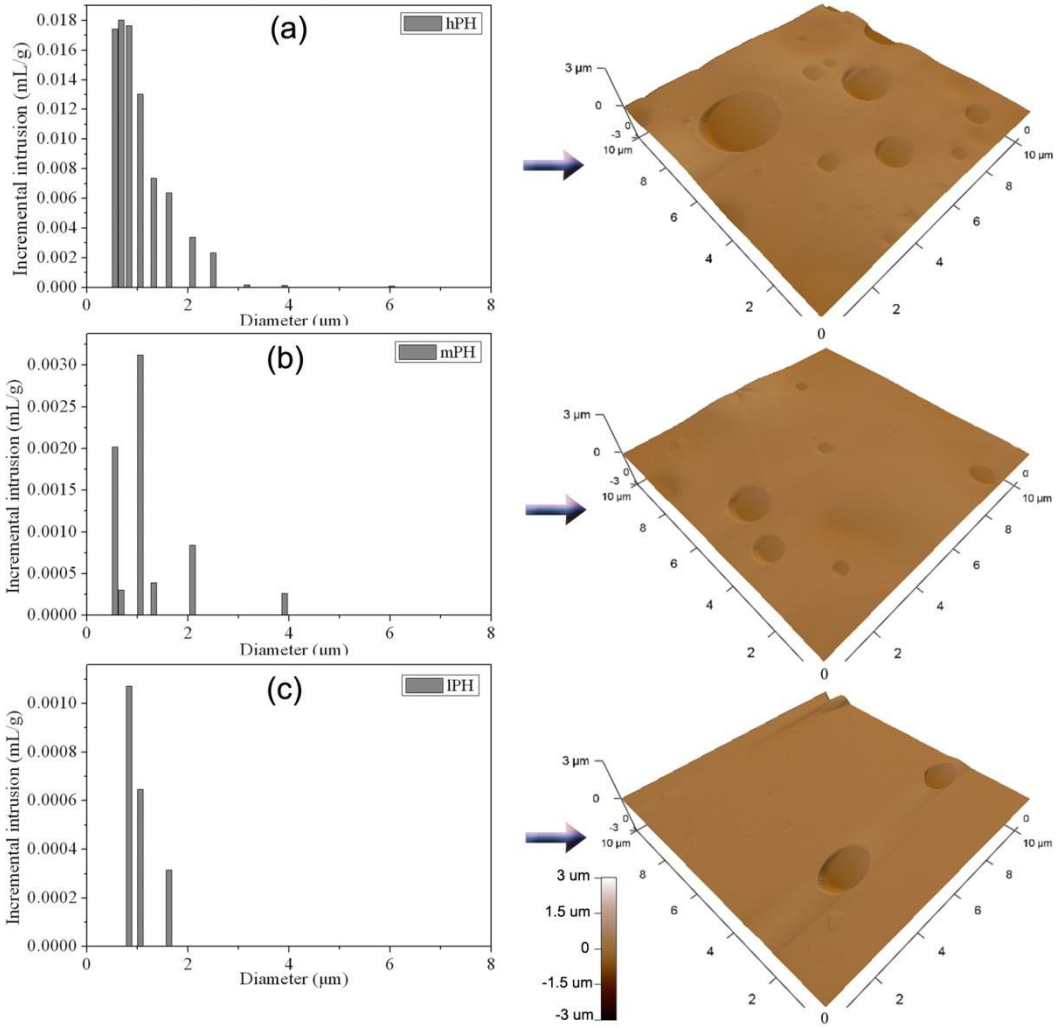

Fig. 4 The size distributions and AFM high-resolution images of macropores on hPH (a), mPH (b) and lPH (c) microspheres.

Mercury intrusion was used to quantitatively compare the features of macropores on different PLGA/HA microspheres. The microspheres were also scanned by AFM to compare the high-resolution details. In Fig. 4, it was seen that the great majority of macropores were below 4 μm. The average sizes of macropores on hPH, mPH and lPH were of 0.99, 1.14 and 1.03 μm, respectively. So the three groups of microspheres had macropores of comparable sizes. The corresponding porosity calculated was 5.13%, 0.48% and 0.14%, respectively. Therefore, the density of macropores that was related to porosity, decreased in the order of hPH, mPH and lPH. The quantitative features of macropores were in line with the SEM observation. The number of macropores also presented a declining trend in AFM as in SEM observation. It could be seen that the features of the non-pores regions in all microspheres were similar. These regions were all smooth and no special changes were observed. The difference in morphologies was mainly caused by the macropores.

3.2. Evolution of Morphology of Microsphere with Degradation

As for degradable materials, surface features might change with degradation. Figure 5 showed the morphology evolution of the three PLGA/HA microspheres. After 5 days of degradation, the closed macropores in hPH basically all opened, which was due to the quick degradation and disappearance of thin film covering the macropores. In contrast, the portion of small macropores in mPH and lPH reduced and the rest macropores enlarged. This was probably the result of volume swelling derived from water adsorption. After 10 days, the portion of small macropores in hPH also reduced and the rest macropores became larger because of obvious swelling. As the degradation and swelling proceeded until 18 days, the size of macropores increased correspondingly. Several HA particles were exposed on mPH after 10 and 14 days of degradation since the HA in mPH had the largest size. The surface of mPH became increasingly rough with degradation. After 18 days, the great swelling further extinguished the macropores and previously exposed HA particles lost. Many fine macropores were present on lPH after 10 days, which were dervied from autocatalysis. The new macropores were extinguished gradually and the surface of lPH also turned rough with degradation. As a whole, the surfaces would turn rough and macropores faded away with degradation.

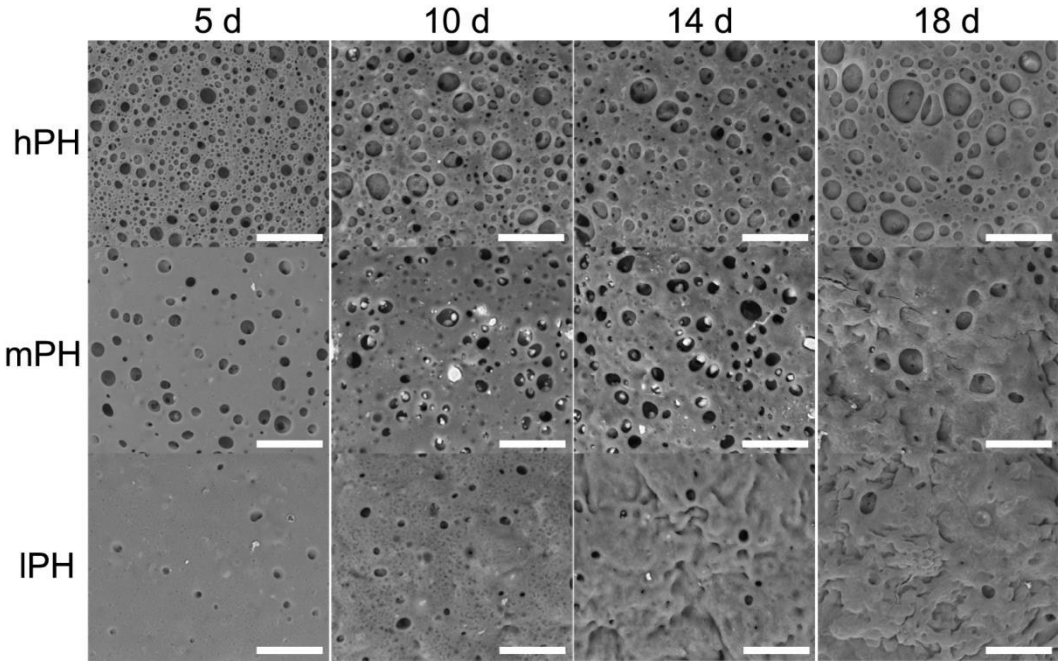

Fig. 5 The morphologies of different PLGA/HA microspheres after *in vitro* degradation in PBS. The white bar was 40 μm.

3.3. Cell Response to PLGA/HA Microspheres

Fig. 6a revealed the Ca^{2+} release from the different PLGA/HA microspheres. hPH and mPH had the similar trend of ion release. The three groups had close release in the early stage, while lPH had higher release in the later stage. Fig. 6b presented the proliferation of fMSCs on the three PLGA/HA microspheres. It was seen that cells grew well with time on all the microspheres, confirming the cytocompatibility of the substrates. It seemed that cells grew best on mPH among the three microspheres. Meanwhile, hPH microspheres were superior to lPH microspheres in proliferation. The result suggested that cell growth responded to the topographic cues of the spherical substrates.

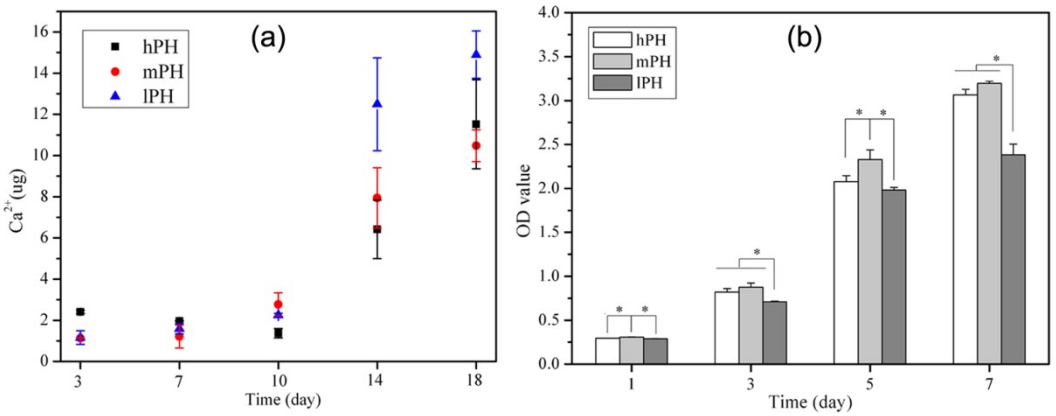

Fig. 6 The Ca^{2+} release from (a) and proliferation of fMSCs on (b) PLGA/HA microspheres with different topographies by CCK-8. The star indicated the significant difference when $p<0.05$.

Fig. 7a showed the morphologies of fMSCs adhering on the three PLGA/HA microspheres. Areas with sparse cells were chosen to clearly observe the cells. The fMSCs spread well on all PLGA/HA microspheres and remained a spindle shape. Since the macropores were much smaller than cell bodies, cells tended to cross over or circumvent the macropores. Cells on hPH seemed more elevated from the surface when compared with those on mPH and lPH. Since it is difficult to distinguish adhering cells from organic substrates in SEM, fMSCs morphologies were also observed by CLSM (Fig. 7b-d). Cell pseudopodia were better identified. As similar to SEM observation, the fMSCs spread well in a spindle shape. However, cells on hPH spread not as flat as on mPH and lPH. Fig. 7g showed the gene expression of fMSCs on PLGA/HA microspheres. ALP, OC and OPN were well-accepted bone markers synthesized by osteoblasts. Although fMSCs had comparable expression of OC on the three groups of microsphere, the expression of ALP and OPN was higher on hPH and mPH than on lPH. And that the hPH and mPH basically presented the similar expression levels of the three genes. This indicated that the osteogenic differentiation of fMSCs on hPH and mPH was comparable, but greater than on lPH.

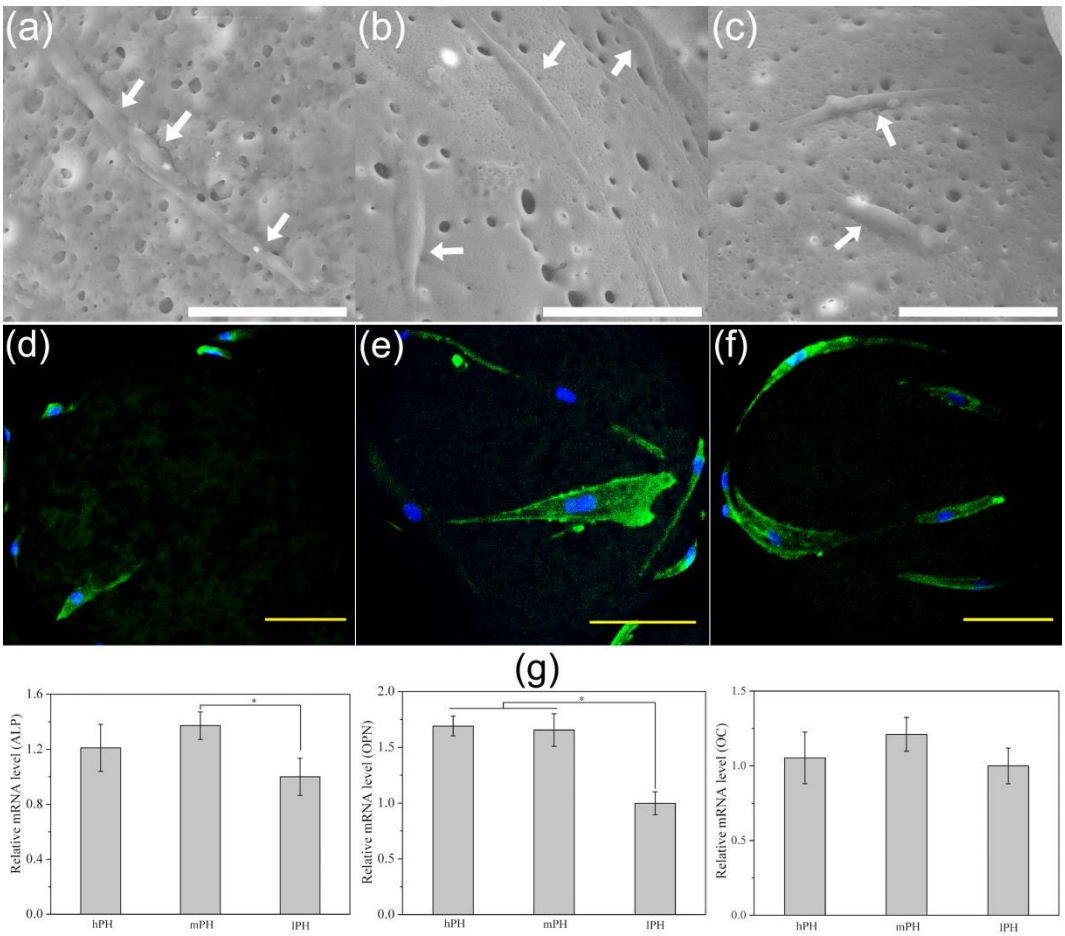

Fig. 7 The morphologies of fMSCs cultured on hPH (a and d), mPH (b and e) and lPH (c and f) microspheres, and the osteogenic gene expression of ALP, OPN and OC (g) after 14 days. Cells in SEM images were indicated by white arrows. The green fluorescence indicated cytoskeletal filamentous actin while blue indicated nuclei. The white bar was 50 μm. The yellow bar was 50 μm. The results were normalized to the lPH group and the star indicated the significant difference when $p<0.05$.

4. Discussion

In this work, PLGA/HA spherical substrates with macroporous surfaces were designed. The arrays of macropores of the microspheres produced an isotropic topography.

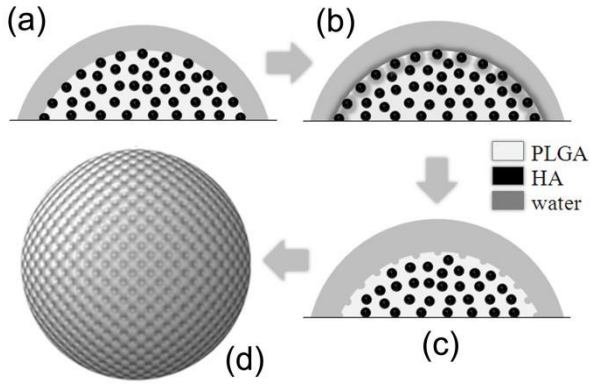

Fig. 8 Formation process of the PLGA/HA microspheres. (a) The PLGA/HA oil droplet in water. (b) The HA attracted water and formed a HA-water-polymer transition around the surface. (c) The exposed HA particles were consumed and left water pockets. (d) Macropores were formed on the surface after drying.

It is reported that nanosized HA could work with salted-out PVA to generate cone-like pores on microspheres around 20 μm in diameter.[19] Our previous work proved that micro-scale calcium carbonate particles could generate macropores in PLGA microsphere via attracting water from aqueous phase near under the surface.[20, 21] In this work, either micro-scale or nano-scale hydrophilic HA particles were also supposed to attract water from the aqueous phase, forming a HA-water-polymer transition zone around the surface (Fig. 8b). This was approved by the superficial macropores and the cavities around HA in PLGA/HA prepared without GAL (Fig. S1c). The water pockets retained in the transition zone turned into the macropores once the oil droplets solidified (Fig. 8c). The exposed HA on the surface would be ultimately dissolved by GDL in the aqueous phase. The GDL removed the exposed HA and facilitated the formation of open macropores.

For large HA particles, the extent of encapsulation by PLGA matrix was not as great as small HA particles. So the large HA particles were easy to protrude and attract water. However, the large HA particles had limited surface area to capture water, resulting in the reduction of the water pockets and thus the macropores (as in mPH).[22] Although nano-HA particles had large surface area, they were more embedded into PLGA, compromising the water-attracting action. So the pore-forming phenomenon of the nano-HA particles was too weak (as in lPH). When the size of the HA was suitable, simultaneously large

enough to be exposed on the surface to attract water and having enough surface area to capture water, a most porous morphology was obtained (as in hPH). Since large HA particles protruded more from the oil droplets, more HA particles would be accordingly consumed by GDL. This explained why more HA was consumed as the size of HA increased in TG result. In fact, if the size of the microspheres was reduced to around 200 μm, the macroporous features of hPH and mPH were enhanced (Fig. S2). This was probably due to the higher specific surface area of smaller microspheres, which facilitated water attraction and even caused confluence of water pockets (Fig. S2a and d). So the morphologies of microspheres were also coupled with the size.

So far, abundant studies have dealt with the cellular responses to patterned surfaces. Diverse isotropic/anisotropic nano-/micro-scale topographies such as grooves, pits and dots have been designed by techniques like polymer lithography and demixing.[23-25] However, shapes of the substrates were confined to planar films or sheets. Although several reports claimed structure similar to 3D via generating physical patterns, the model substrates were essentially far from 3D.

In this work, arrays of macropores were achieved on spherical substrates. Several studies reported that cells would respond to macropores of several micrometers.[7, 8] It is also proved that Ca^{2+} release contributed to proliferation and osteogenic differentiation of cells.[26, 27] As shown in Fig. 7a, the three groups of microspheres had close ion release, confirming that topography was the main factor affecting cell proliferation. Our result demonstrated that fMSCs preferred to proliferate on spherical substrate with medium density of macropores than on substrate having the most macropores. This was possibly because more pores would aggravate the surface discontinuity that inhibited cell proliferation.[7] It was believed that different topographies exhibited different roughness. Several studies proved that rough surface could facilitate proliferation of bone marrow stem cells.[28, 29] Here hPH microspheres were supposed to have the highest roughness, while lPH the lowest. This explained why fMSCs grew better on hPH than on lPH. Cells on hPH were not as flattened as on mPH and lPH. Y. Khung *et al.* also found that cells would resist attachment and flattening on a porous substrate.[30] This might be because cells were hard to form circumferential actin filament over macropores.

The effect of topography on gene expression of cells was also extensively studied. For instance, X. Shi *et al.* proved that introducing topographic cue (grooved micropattern) into scaffold could promote the osteogenesis of human MSCs.[31] Slightly disordered arrays of nanopits also induced MSCs to produce bone mineral *in vitro*.[32] Our results demonstrated that arrays of macropores on microspheres did influence osteogenic differentiation of fMSCs. Although lPH had a higher ion release at the later stage, cells on hPH and mPH still exhibited stronger sign of osteogenic differentiation. This further highlighted the role of topography in influencing cell activities. Isotropic topography, as the macropores on the microspheres, was supposed to influence the collective behaviors such as proliferation and differentiation of cells.[33] The different features of macropores were sensed by cell surface receptors and integrated by intracellular signaling pathways, which regulated the gene expression and the ultimate cell phenotype.[34] Unlike conventional planar substrates, the substrates used were 3D hybrid microspheres that were more applicable in bone repair. Combined with the performance on both proliferation and osteogenic differentiation, PLGA/HA microspheres with medium-density arrays of macropores were considered to be the most beneficial for fMSCs. It should be noted that the surface feature of biodegradable devices, as proved in Fig. 5, would change great with degradation. The conclusion merely referred to the initial state of the surface feature.

5. Conclusions

In summary, we produced arrays of macropores on PLGA/HA, generating a 3D topography. Different sizes of HA generated different spherical topographies. Culturing fMSCs on microspheres revealed that microspheres possessing medium density of macropores performed best in terms of proliferation and osteogenic differentiation of the fMSCs. Our finding may be of use in understanding substrate-cell interaction and designing more powerful devices for bone repair. Future study is to study the synergetic effects of microsphere size and surface morphologies on cells.

Acknowledgements

This study was financially supported by National Basic Research Program of China (2012CB619100, 2011CB606204), National Natural Science Foundation of China (51372085), the Specialized Research Fund for the Doctoral Program of Higher Education of China (20110172120002), Science and Technology Program of Guangdong Province (2012A061100002), Program for New Century Excellent Talents in University (NCET-11-0148), the 111 Project (B13039) and Fundamental Research Funds for the Central Universities (2013ZZ0005).

Notes and references

[a] School of Materials Science and Engineering, South China University of Technology, Guangzhou 510641, China.
[b] National Engineering Research Center for Tissue Restoration and Reconstruction, Guangzhou 510006, China.
[c] Guangdong Province Key Laboratory of Biomedical Engineering, South China University of Technology, Guangzhou 510006, China.

Electronic Supplementary Information (ESI) available: SEM images of PLGA/HA microspheres prepared without GDL in the aqueous phase. See DOI: 10.1039/b000000x/

1. N. M. Alves, I. Pashkuleva, R. L. Reis and J. F. Mano, *Small*, 2010, **6**, 2208-2220.
2. D. Cheng, X. Cao, H. Gao, X. Ye, W. Li and Y. Wang, *RSC Adv.*, 2014, **4**, 9031-9038.
3. S. Hoon áAhn, H. Jong áLee, U. Seok áChung and J. Hak áKim, *RSC Adv.*, 2013, **3**, 23673-23680.
4. B. D. Boyan, T. W. Hummert, D. D. Dean and Z. Schwartz, *Biomaterials*, 1996, **17**, 137-146.
5. C. Wilkinson, M. Riehle, M. Wood, J. Gallagher and A. Curtis, *Mater. Sci. Eng., C*, 2002, **19**, 263-269.
6. Y. Wan, Y. Wang, Z. Liu, X. Qu, B. Han, J. Bei and S. Wang, *Biomaterials*, 2005, **26**, 4453-4459.
7. S. J. Lee, J. S. Choi, K. S. Park, G. Khang, Y. M. Lee and H. B. Lee, *Biomaterials*, 2004, **25**, 4699-4707.
8. C. C. Berry, G. Campbell, A. Spadiccino, M. Robertson and A. S. Curtis, *Biomaterials*, 2004, **25**, 5781-5788.
9. G. Li, Q. Shi, S. Yuan, K. Neoh, E. Kang and X. Yang, *Chem. Mater.*, 2010, **22**, 1309-1317.
10. G. L. Li, H. Möhwald and D. G. Shchukin, *Chem. Soc. Rev.*, 2013, **42**, 3628-3646.
11. M. Li, G. L. Li, Z. Zhang, J. Li, K.-G. Neoh and E.-T. Kang, *Polymer*, 2010, **51**, 3377-3386.
12. X. Shi, L. Ren, M. Tian, J. Yu, W. Huang, C. Du, D.-A. Wang and Y. Wang, *J. Mater. Chem.*, 2010, **20**, 9140.
13. X. Shi, Y. Wang, L. Ren, N. Zhao, Y. Gong and D. A. Wang, *Acta Biomater.*, 2009, **5**, 1697-1707.

14. W. Xu, L. Wang, Y. Ling, K. Wei and S. Zhong, *RSC Adv.*, 2014, **4**, 13495-13501.
15. M. R. Rogel, H. Qiu and G. A. Ameer, *J. Mater. Chem.*, 2008, **18**, 4233-4241.
16. C. J. Bettinger, R. Langer and J. T. Borenstein, *Angew. Chem. Inter. Ed.*, 2009, **48**, 5406-5415.
17. X. Shi, S. Chen, J. Zhou, H. Yu, L. Li and H. Wu, *Adv. Funct. Mater.*, 2012, **22**, 3799-3807.
18. F. J. O'Brien, *Materials Today*, 2011, **14**, 88-95.
19. C. Takai, T. Hotta, S. Shiozaki, Y. Boonsongrit and H. Abe, *Chem. Commun.*, 2009, 5533-5535.
20. D. Cheng, X. Cao, H. Gao and Y. Wang, *J. Mater. Chem. B*, 2013, **1**, 3322-3329.
21. D. Cheng, H. Gao, L. Hao, X. Cao and Y. Wang, *Mater. Lett.*, 2013, **111**, 238-241.
22. D. Cheng, X. Cao, H. Gao and Y. Wang, *RSC Adv.*, 2013, **3**, 6871-6878.
23. M. Dalby, S. Childs, M. Riehle, H. Johnstone, S. Affrossman and A. Curtis, *Biomaterials*, 2003, **24**, 927-935.
24. S. Kelleher, Z. Zhang, A. Löbus, C. Strehmel and M. Lensen, *Biomater. Sci.*, 2014, **2**, 410-418.
25. N. Y. Lee, *Colloids Surf., B*, 2013, **111**, 313-320.
26. S. Maeno, Y. Niki, H. Matsumoto, H. Morioka, T. Yatabe, A. Funayama, Y. Toyama, T. Taguchi and J. Tanaka, *Biomaterials*, 2005, **26**, 4847-4855.
27. H. Matsuoka, H. Akiyama, Y. Okada, H. Ito, C. Shigeno, J. Konishi, T. Kokubo and T. Nakamura, *J. Biomed. Mater. Res.*, 1999, **47**, 176-188.
28. X. Hu, S.-H. Park, E. S. Gil, X.-X. Xia, A. S. Weiss and D. L. Kaplan, *Biomaterials*, 2011, **32**, 8979-8989.
29. T. Osathanon, K. Bespinyowong, M. Arksornnukit, H. Takahashi and P. Pavasant, *J. Oral Sci.*, 2011, **53**, 23-30.
30. Y. Khung, G. Barritt and N. Voelcker, *Exp. Cell Res*, 2008, **314**, 789-800.
31. X. Shi, S. Chen, Y. Zhao, C. Lai and H. Wu, *Adv. Healthcare Mater.*, 2013, **2**, 1229-1235.
32. N. Gadegaard, M. J. Dalby, M. O. Riehle and C. D. Wilkinson, *J. Vac. Sci. Technol., B: Microelectron. Nanometer Struct.*, 2008, **26**, 2554-2557.
33. J. Y. Lim and H. J. Donahue, *Tissue Eng.*, 2007, **13**, 1879-1891.
34. M. Lutolf and J. Hubbell, *Nat. Biotechnol.*, 2005, **23**, 47-55.

